Comparison of kilometric continuum latitudinal radiation patterns with linear mode conversion theory

Scott A. Boardsen,[1,2] James L. Green,[3] and Bodo W. Reinisch[4]

Received 3 February 2007; revised 10 October 2007; accepted 6 November 2007; published 31 January 2008.

[1] Using 80 observations of kilometric continuum (KC) radiation patterns detected by the Radio Plasma Imager on the IMAGE spacecraft, the latitudinal variation of these radiation patterns is compared with the predictions of linear mode conversion theory (LMCT). Six of these comparisons are presented in this paper. Because the location and shape of the plasmapause at the source cannot be simultaneously determined with all of the KC observations, we estimated the minimum frequency-dependent beaming angle possible based on a statistical upper limit plasma density versus *L*-shell profile. This density versus *L*-shell profile is equated to the 90th percentile plasma density versus *L*-shell curve derived from over 40,000 in situ measurements of the upper hybrid resonance frequency made over the first 3 years of the IMAGE mission. For all cases, starting at frequencies approximately >150 kHz, the model beam center was found to lie just within or outside the radiation pattern. Unrealistic peak densities are required at the equatorial source *L*-shell locations which are necessary to force the beam centers to lie deep within the observed radiation patterns. We present this as strong evidence that LMCT cannot be used to explain KC. In order to explain the latitudinal location of the high-frequency end of these KC radiation patterns a theory is required in which these frequencies are beamed at equatorial angles that are much smaller than the predictions of LMCT. Hashimoto et al. (2005), analyzing one KC radiation pattern detected by CRRES, reached the same conclusion. We present one case in which the source location was inferred by equating the harmonic spacing in the KC radiation pattern with the model electron cyclotron frequency at the source. The LMCT model beams, for this source location, were found to lie outside of the radiation pattern at all frequencies, again consistent with Hashimoto et al. (2005). In addition a survey of KC observations by IMAGE in MLT is presented in which the probability of occurrence peaks in both the dawn and evening sectors.

Citation: Boardsen, S. A., J. L. Green, and B. W. Reinisch (2008), Comparison of kilometric continuum latitudinal radiation patterns with linear mode conversion theory, *J. Geophys. Res.*, *113*, A01219, doi:10.1029/2007JA012319.

1. Introduction

[2] The Earth's nonthermal continuum radiation is observed from 10 to 800 kHz [see, e.g., *Gurnett*, 1975; *Hashimoto et al.*, 1999]. At frequencies less than the magnetopause plasma frequency (~30 kHz) the continuum radiation has been referred to as the "trapped" component [*Gurnett and Shaw*, 1973]. At frequencies above the magnetopause plasma frequency the emission has been referred to as the "escaping" component [*Kurth et al.*, 1981]. Continuum in the frequency range of 100 kHz to 800 kHz, whose source is near the magnetic equator of the inner magnetosphere, was first identified by *Hashimoto et al.* [1999] as an emission distinct from nonthermal continuum radiation (NTC) [*Gurnett*, 1975] whose frequency range is primarily from ~5 kHz to 100 kHz. Hashimoto called this radiation kilometric continuum (KC) suggesting that KC was more than just the high-frequency extension of NTC. This term was coined for two reasons: (1) the high-frequency extent suggested a source deep within the equatorial plasmasphere while NTC originates near or at the equatorial plasmapause and (2) KC occurs at all magnetic local times, while direction finding of NTC shows that its source is primarily in the dawn sector [*Gurnett*, 1975]. As opposed to KC originating from deep within the plasmasphere, there is now strong evidence that KC does originate from the plasmapause inside structures like notches and shoulders [*Green et al.*, 2002, 2004]. For reviews of KC, see *Hashimoto et al.* [2006] and *Green and Boardsen* [2006]. The radiation

[1]Goddard Earth Sciences and Technology Center, University of Maryland, Baltimore County, Baltimore, Maryland, USA.
[2]Also at Space Weather Laboratory, Heliophysics Science Division, NASA Goddard Space Flight Center, Greenbelt, Maryland, USA.
[3]Planetary Sciences Division, NASA Headquarters, Washington, D. C., USA.
[4]Center for Atmospheric Research, University of Massachusetts-Lowell, Lowell, Massachusetts, USA.

Copyright 2008 by the American Geophysical Union.
0148-0227/08/2007JA012319

pattern of KC is often observed to extend downward in frequency into the upper portion of the NTC frequency range.

[3] The radiation patterns of both KC and escaping NTC [*Kurth et al.*, 1981] have large longitudinal extents and they often exhibit harmonics in their frequency spectra. Therefore it is believed that they are generated by the same mechanism. In the mid-1980s, linear mode conversion theory (LMCT) [*Jones*, 1976, 1980, 1981; *Budden*, 1980, 1986; *Budden and Jones*, 1987] became the accepted explanation of NTC. In LMCT, electrostatic waves, generated by unstable electron distributions, are transformed into *Z*-mode radiation as the waves propagate; when the *Z*-mode radiation reaches the radio window it mode converts into the *L-O* free space mode. The key prediction of LMCT is that free space radiation emerging from the radio window will form two symmetrical beams about the magnetic equator whose beaming angles in latitude are given by, $\pm\tan^{-1}\sqrt{f_{ce}/f_{pe}}$ where the wave frequency is equal to the plasma frequency (f_{pe}) at the radio window, and f_{ce} is the electron cyclotron frequency at the radio window. The gradual acceptance of LMCT as the best explanation for NTC was due to studies like that of *Horne* [1989], who showed that the original electrostatic waves can reach the radio window without being sufficiently damped out as they propagate to the window radio and from observations of the beaming of free space mode radiation from the window [*Jones et al.*, 1987; *Jones*, 1988].

[4] Further testing of the symmetrical beaming prediction of LMCT was made in a comprehensive study by *Morgan and Gurnett* [1991]. At frequencies primarily below 100 kHz the location of the source region was estimated by planar direction finding using one spacecraft (Dynamics Explorer-1) at different positions along its orbit. *Morgan and Gurnett* [1991] presented 11 events in Table 1 of their paper in which beaming angles where estimated from direction finding and compared against the predictions of LMCT. Eleven of the nine events occurred at frequencies less than 100 kHz. Two occurred in the KC range but below 150 kHz. Of these 11 events, for three the range of inferred beaming angles overlapped the range of predicted beaming angles, for one the range of inferred beaming angles was less than the range of predicted beaming angles, and in seven the range of inferred angles were greater than the range of predicted angles. They also noted that in general a two beam pattern about the magnetic equator was not observed. *Morgan and Gurnett* [1991] concluded that the LMCT beaming angle formula is a "poor predictor of the observed beaming." However, they acknowledge that their conclusions are partially mitigated by radiation of solar origin which maybe interfering with direction finding for some of their cases and that source of the radiation is probably extended in space.

[5] The lack of an observed two beam pattern in itself cannot rule out LMCT because there are many factors that could contribute to the smearing out and spreading out this pattern, for example, (1) overlap of the two beam widths, (2) an extended source region in longitude that is not coplanar, (3) an extended source region in latitude about the magnetic equator, and (4) the waving of the ambient background magnetic field direction at the source from low-frequency transverse Alfven waves. All of these factors, however, would tend to broaden the radiation pattern in latitude rather than narrow it.

[6] *Hashimoto et al.* [2005] analyzed a KC event (from 0010 to 0230 UT on 7 September 1990) observed in the CRRES wave data for which the source location was taken to be at an *L*-shell of 3.9 Earth radii (R_E), the *L*-shell where CRRES crossed the plasmapause (outbound at 2245 UT, 6 September) approximately 90 min before encountering these emissions. Using this equatorial source location, Hashimoto then compared the observed beaming angles with the LMCT predicted beaming angles. He found that the observed angles are significantly smaller than the theoretical values by as much as $\sim 8°$ and concluded that the inferred plasmapause position would have to be at 4.3 R_E rather than 3.9 R_E to make the LMCT predictions consistent with observations. Like *Morgan and Gurnett* [1991], Hashimoto could see no evidence of a symmetrical two beam structure in the radiation pattern as the spacecraft transversed the magnetic equator. Examining the Upper Hybrid Resonance (UHR) line in the spectrogram from Figure 4 of *Hashimoto et al.* [2005], it looks like CRRES crossed the plasmapause inbound around 0530 UT at a dipole *L*-shell of 4.4 R_E. Outbound, there is a sudden transition in gradient from the plasmasphere to plasmapause around 200 kHz, whose effects are not observed in the KC event around the same frequency. Thus even for this example, the source location is inferred and not based on simultaneous observations of the plasmapause during detection of the KC radiation.

[7] The purpose of this paper is to examine the radiation patterns of the high-frequency portions (above 100 kHz) of NTC events. All these events have peak emission frequencies >100 kHz, well above the magnetopause plasma frequency, and as such are referred to as kilometric continuum (KC). We note that KC is most likely equivalent to the high-frequency end of escaping continuum. In this paper we present a statistical survey of KC observed by the Radio Plasma Imager (RPI) on the IMAGE spacecraft. A similar survey was made by *Hashimoto et al.* [1999] using data from the Plasma Wave Instrument on the Geotail spacecraft. This survey of *Hashimoto et al.* [1999] was performed at much larger radial distances from the source ($\sim$6 to $\sim$24 R_E) due to Geotail's orbit and emission "hot spots" in magnetic local time (MLT) can be smeared out and not observed due to the large longitudinal angular width of this radiation. IMAGE whose orbit places it much closer ($\sim$3 R_E) to the plasmaspheric source region during equatorial crossings is in a much more favorable position to observe variations in source activity with MLT.

[8] Using RPI data, we further investigate the validity of LMCT when used to explain KC. We compare the observed KC radiation pattern for 80 events with the predications of LMCT using methods similar to that of *Hashimoto et al.* [2005]. Six of these comparisons, of the latitudinal variation of KC, are presented here. In one of these a clear harmonic signature is present in the KC, from which the source location is inferred by equating the harmonic spacing with the magnetic dipole model derived f_{ce} at the source. For all of the events presented in this paper it is clear that LMCT theory fails to adequately explain the latitudinal pattern of KC because unreasonably high plasma densities would

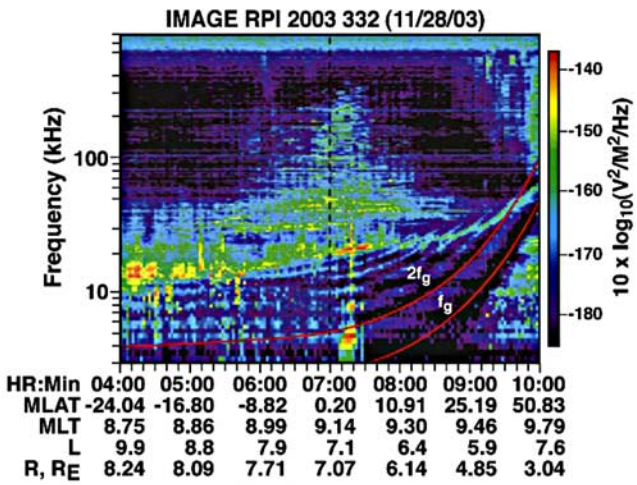

Figure 1. Example of a typical kilometric continuum (KC) radiation pattern, peaking near 400 kHz shortly after 0700 UT, observed by Radio Plasma Imager (RPI) on the IMAGE spacecraft as it latitudinally transverses the Earth's magnetic equator. We coined the term "Christmas tree" to describe the shape of this pattern as observed in frequency-time spectrograms. The dashed vertical line shows the location of the dipole equator.

be required at the source L-shell necessary to force the LMCT beams to lie within the observed radiation pattern.

2. Description of Orbit, Instrument, and Data Set

[9] The IMAGE spacecraft [*Burch*, 2000] is in a polar orbit with apogee of $\sim$8.25 R_E and a perigee of $\sim$1.10 R_E, and its orbital period is $\sim$14.23 h. This orbit is ideal for studying the latitudinal variation of KC. The spacecraft spin axis is oriented perpendicular to the orbit plane and the spin period is $\sim$2 min. The RPI instrument [*Reinisch et al.*, 2000] on the IMAGE spacecraft was designed to operate in both an active mode and a passive mode. In the active mode RPI transmits radio pulses and listens for their return echoes [*Galkin et al.*, 2004]. In the passive mode RPI operates as a sensitive receiver and samples the natural magnetospheric emissions. The passive measurements are used in this study. The signals from the three orthogonal electric field antennas on IMAGE are simultaneously sampled by the RPI receiver. The 20 m tip-to-tip E_Z antenna is aligned along the spacecraft's spin axis, while the two 500 m tip-to-tip E_X and E_Y antennas are in the spin plane. The long spin plane antennas were shortened (attributed to collisions with micrometeorites) near the fall eclipse seasons. The combined electric field intensity from the E_X and E_Y dipole antennas are used in this study. The measurements made by the E_Z dipole antenna are not used in this study.

[10] In the passive mode RPI was programmed to make two frequency sweeps; a 3 kHz to 20 kHz sweep composed of 44 linearly spaced frequency steps over 10 s, followed immediately by a 20 kHz to 1 MHz sweep composed of 198 logarithmically spaced frequency steps over 50 s. Owing to instrument operations using the active mode the cycle times between complete sweeps in frequency was about 2 1/2 min. The bandwidth of each measurement is 300 Hz.

[11] The RPI passive mode data set, used in this study, covered the period from May 2000 to January 2004. Frequency-time spectrograms of the combined E_X and E_Y electric field measurements where generated for all crossings of the magnetic equator by IMAGE and these spectrograms were visually examined for KC.

3. Observations

[12] An example of a KC radiation pattern detected as IMAGE latitudinally transverses the magnetic equator is shown in the frequency-time spectrogram in Figure 1. As IMAGE approaches the magnetic equator, first the low frequencies of this emission are encountered followed by higher frequencies, peaking around 400 kHz near the true magnetic equator at 0719 UT (indicated by the brief enhancement of presumably electrostatic emissions at lower frequencies between 3 and 30 kHz). As IMAGE moves away from the equator the opposite trend in frequency occurs. Since this radiation pattern observed in the spectrogram resembles a "Christmas tree," we coined this term to describe this type of pattern. This term was first used in the review paper by *Green and Boardsen* [2006]. A similarly shaped KC radiation pattern is shown in Figure 4 of *Hashimoto et al.* [2005] from 0010 to 0230 UT on 7 September 1990.

[13] Four other examples of KC radiation patterns detected by RPI during magnetic equator crossings by IMAGE are shown in Figures 2a–2d. The white curve superimposed on each figure is the beam center derived from LMCT using the 90th percentile density versus L-shell relation and will be discussed in the following section. We define the beam center as the beam formed by the free-space radiation emerging from the center of the radio window. Figure 2b was presented in the review by *Green and Boardsen* [2006] with an orbit insert. The radiation patterns in Figures 2b and 2c were detected in the dawn sector, while the radiation patterns in Figures 2a and 2d were detected in the midafternoon and dusk sectors, respectively. In most of the KC observations by IMAGE there is no distinct transition in the observed radiation patterns across the $\sim$100 kHz demarcation frequency between "KC" and "NTC" radiation. Only in Figure 2a is there possible evidence of a two lobe structure and it occurs at frequencies less than $\sim$100 kHz where there is a diminishing of intensity as the magnetic equator is crossed. These two lobes (or beams), as would be qualitatively predicted by LMCT, merge at frequencies above $\sim$100 kHz. In the other patterns the emissions appear more or less smooth across the equator with little evidence of being composed of two lobes. In our survey we have found four events in which the radiation pattern could be interpreted as being composed of two lobes centered about the magnetic equator. In all of these cases the lobe structures were observed at frequencies less than 100 kHz.

[14] We manually examined 1700 magnetic equator crossings by IMAGE for KC events and identified around 140 crossings in which KC was detected. The IMAGE observations of KC are made when the spacecraft is typically between 2.5 and 8.3 R_E, with a median of 6 R_E.

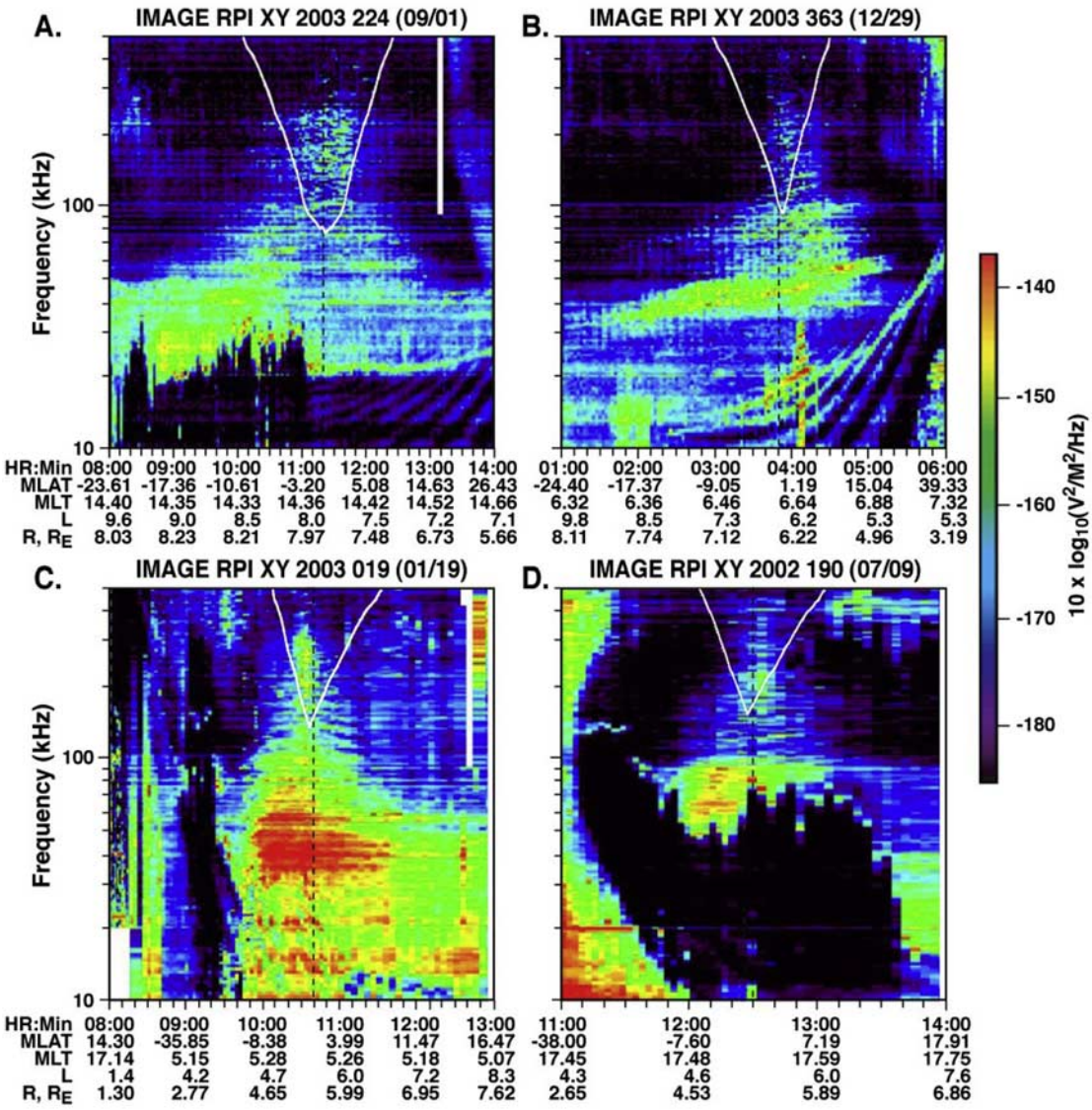

Figure 2. (a–d) Examples of KC radiation patterns observed by RPI as IMAGE transverses latitudinally through the magnetic equator. A two lobe pattern (or diminishing of emission intensity below 100 kHz around the equator) can be seen in Figure 2a. The white curve is the center of the LMCT beams derived from the 90th percentile plasma density curves (Figure 7). For LMCT to be correct these curves should lie deep within the radiation pattern at all frequencies but instead lie outside the pattern at the high-frequency end of the emission.

The distribution of the 1700 equatorial crossings by IMAGE is shown in the scatterplot of Figure 3. The azimuthal coordinate is magnetic local time (MLT), while the radial coordinate is equatorial *L*-shell. The black dots correspond to crossings in which no KC was detected and the red dots correspond to crossings in which KC was detected. The frequency of occurrence for detecting KC with MLT is shown in Figure 4. The dropout from 1400 to 1600 MLT is due to small sampling in that range. KC is observed at all MLTs, consistent with Geotail observations of KC [*Hashimoto et al.*, 1999; *Green et al.*, 2004] but is strongly peaked in the dawn sector with a secondary peak in the dusk sector as shown Figure 4 in contrast with the more smoothly varying frequency of occurrence with MLT observed by Geotail. We suspect this difference is due to the broad latitudinal radiation pattern that is associated with KC which may washout the MLT dependence at large distances from the plasmapause of ~6 to ~24 R_E for Geotail; as opposed to ~2 to ~3 R_E for IMAGE. Also since IMAGE, when near the magnetic equator, is closer in it will be outside of the AKR emission cone for a larger percentage of the time compared to that of Geotail for the dusk and midnight sectors. The dawnside peak of the KC occurrence frequency, in this paper, is consistent with the observed dawnside peak of intensity for NTC observed by *Gurnett* [1975]. We speculate that the smaller dusk side peak may be associated with plasmaspheric plumes and that density gradients on the inner edge of the plume tap a free energy source that does

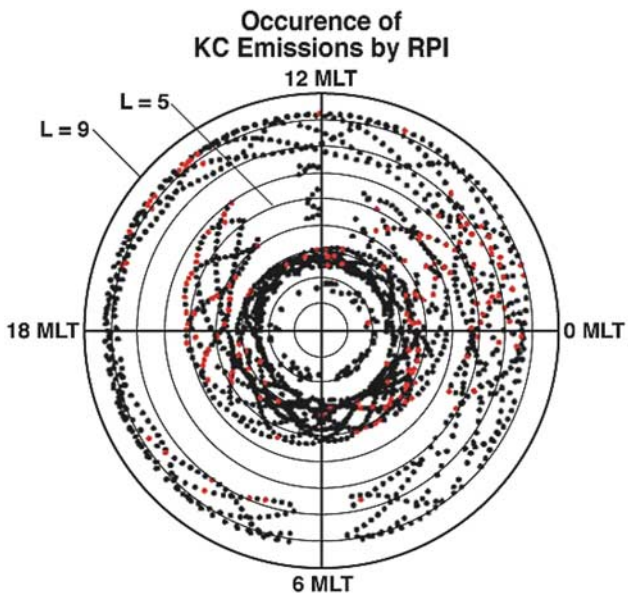

Figure 3. A dial plot in magnetic local time (MLT) (azimuthal coordinate) versus *L*-shell (radial coordinate) of 1700 IMAGE spacecraft equatorial crossings used in this study. The black dots are crossings in which no KC was detected, whereas the red dots indicate the 140 crossings in which KC was detected. The concentric circles are spaced at unit intervals of *L*-shell.

not normally extend inwards to the nominal plasmapause in the dusk sector.

4. Comparison of Observations With LMCT Beaming Formula

[15] LMCT predicts that free space mode radiation (primarily in the L-O mode) will emerge from the radio window where Z-mode waves can be directly converted into free space L-O mode waves or vice versa. The center of the radio window occurs at a point where the wave frequency is equal to the plasma frequency and its wave vector is either parallel or antiparallel to the ambient magnetic field. The transmission coefficient is unity at the center of the window but drops off rapidly away from the window center. A plasma density gradient is required and its magnitude strongly affects the size of the window (the solid angle about the window center where the transmission coefficient is sufficiently large), the larger the gradient the larger the window. As the emerging L-O mode wave propagates away from the window, its wave vector is rapidly refracted away from the ambient magnetic field direction toward the gradient direction. In addition, owing to the strong plasma density gradient, the index of refraction rapidly approaches unity as the wave propagates away from the plasmasphere into lower-density media. This process can be described by a beaming formula. *Budden* [1980, 1986] developed such a radio-window beaming formula for arbitrary angles between the ambient magnetic field and the plasma density gradient direction.

[16] *Jones* [1976, 1980, 1981] and *Jones et al.* [1987] applied the theory of the radio window to explain NTC. He assumed the window is located at the equatorial plasmapause and the plasma density gradient is nearly perpendicular to the ambient magnetic field. Under these assumptions, Budden's beaming angle formula simplifies to that given in the introduction. This formula predicts that two symmetric beams should emerge from the source at the magnetic equator, one at higher latitudes and the other at lower latitudes, where the beaming angle is a function of the f_{ce}/f_{pe} ratio at the source. The wave frequency equals f_{pe} at the radio window. For a fixed f_{ce} the beaming angle decreases as f_{pe} increases. For a KC observation at a given frequency (which fixes f_{pe} at the source), f_{ce} must be decreased (i.e., moving the source radially outward) in order to reduced the predicted beaming angle out of the equatorial plane.

[17] For a sharp plasmapause, where the variation of f_{ce} is small compared to the variation of f_{pe} across the plasmapause, *Hashimoto et al.* [2005] showed how the beaming formula can be used to qualitatively explain the shape of the observed radiation pattern in CRRES plasma wave observations [see *Hashimoto et al.*, 2005, Figures 5 and 6]. Using the beaming formula with f_{ce} nearly constant across the plasmapause, the higher-frequency waves will be beamed at angles closer to the equatorial plane than that of lower-frequency waves. This pattern is illustrated in Figure 5 (similar to Figure 5 of *Hashimoto et al.* [2005]) in which frequency-dependent beams (red traces) were emitted from an equatorial model plasmapause located at a *L*-shell of 3.5 R_E. The IMAGE orbit (black trace) for the event of Figure 1 is overlaid. As IMAGE moves inbound toward the equator first the low frequencies and then high frequencies are encountered, the opposite occurs outbound from the equator. By marking off in time when the spacecraft encounters a particular frequency a simulated frequency-time spectrogram can be created of the beam centers. A simulated spectrogram, for the event shown in Figure 1, of beam centers for different source plasmapause locations of

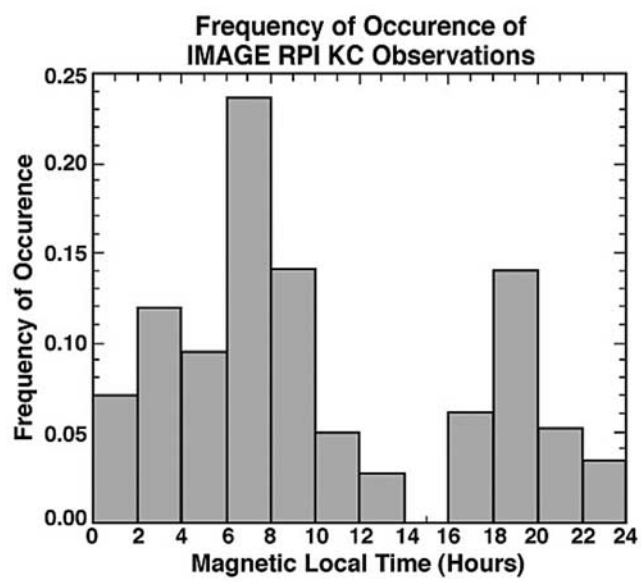

Figure 4. Frequency of occurrence of KC radiation detected by RPI on IMAGE versus MLT for the 1700 magnetic equatorial crossing used in this study.

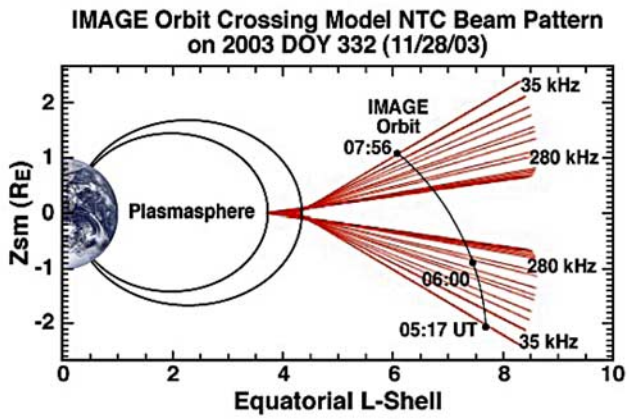

Figure 5. Rays (red curves), whose frequencies varied between 35 and 280 kHz, launched from an equatorial source region for a plasmapause located at 3.5 R_E. A portion of the IMAGE orbit (black curve) corresponding to the spectrogram of Figure 1 is overlaid. The intersection of these rays, whose beaming angles are frequency-dependent with the IMAGE orbit, were used to simulate the spectrograms of Figure 1 for different source plasmapause locations.

2.2, 3.5, and 4.5 R_E is shown in Figure 6. The beams centers for a plasmapause of 2.2 and 3.5 R_E lie well outside of the observed KC emissions of Figure 1, while the beam centers for a plamapause of 4.5 R_E just touches the outer edge of the observed KC emissions. The empirical plasmapause model (which is MLT and K_{Pmax12} dependent) given in Table 1 of *Moldwin et al.* [2002] predicts a plasmapause location at an L-shell of 4.32 ± 0.22 R_E for the MLT sector in which IMAGE was located for the event of Figure 1.

[18] In order to be consistent with LMCT the model beam centers should lie deep within the observed pattern. In order to force the observed beam centers to lie within the observed pattern, for this event, the plasmapause has to be moved outward while the f_{pe} drop across the plasmapause must still encompass the observed frequency range making up the radiation pattern. Note that the peak frequency of the beam centers shown in Figure 6 drop in frequencies as the plasmapause moves outward. Using an empirical density model like *Gallagher et al.* [2000] or *Carpenter and Anderson* [1992] as one moves the plasmapause outward, in order to force beam centers to lie within the radiation pattern, the maximum plasma frequency at the plasmapause drops below the maximum frequency observed in the KC radiation pattern no matter how the parameters in these models are adjusted.

[19] A question arises as to whether the maximum plasma density drop across the plasmapause is realistic for the necessary plasmapause location to force consistency between the observations and LMCT. In lieu of simultaneous direct measurements of the plasmasphere and plasmapause equatorial plasma densities during the detection of KC radiation patterns, we argue that the required maximum plasma density at the necessary source L-shell is statistically unlikely. In order compute the maximum observed plasma density versus L-shell we use a data set of 40,000 in situ plasma density measurements made from RPI passive measurements over the first 3 years of the IMAGE mission [*Fung et al.*, 2001; *Garcia et al.*, 2003]. Figure 7 is a

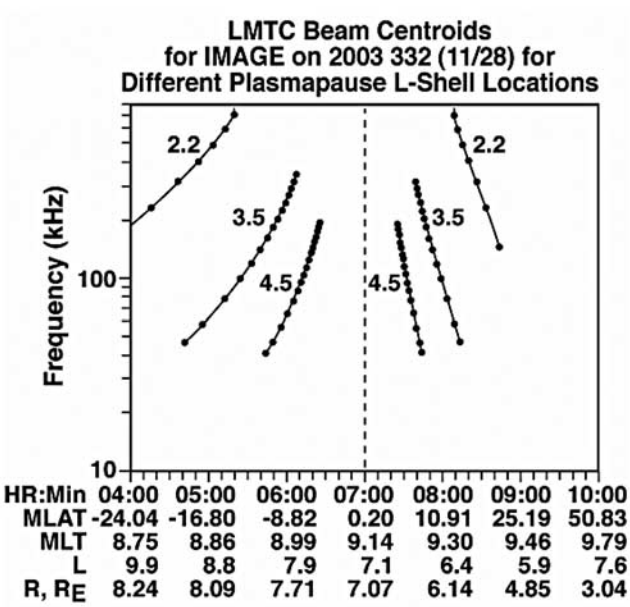

Figure 6. Reconstructed spectrograms of the beam centers for equatorial source (radio window) plasmapause locations of 2.2, 3.5, and 4.5 R_E using the IMAGE orbit shown in Figure 5 corresponding to the observed spectrogram of Figure 1. The dots on each curve are where $f_{pe} = (n + 1/2) f_{ce}$ at the equatorial source.

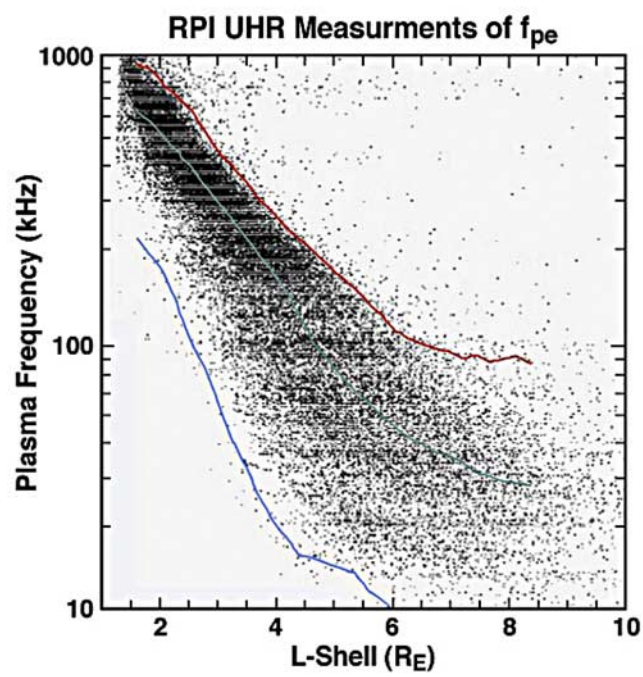

Figure 7. Scatterplot of in situ density measurements versus L-shell. The densities are derived from passive mode upper hybrid resonance measurements by RPI over a 3 year period. The red, green, and blue traces are at the 90th, 50th (median), 1 percentiles that were computed by binning the density measurements into bins of L-shell.

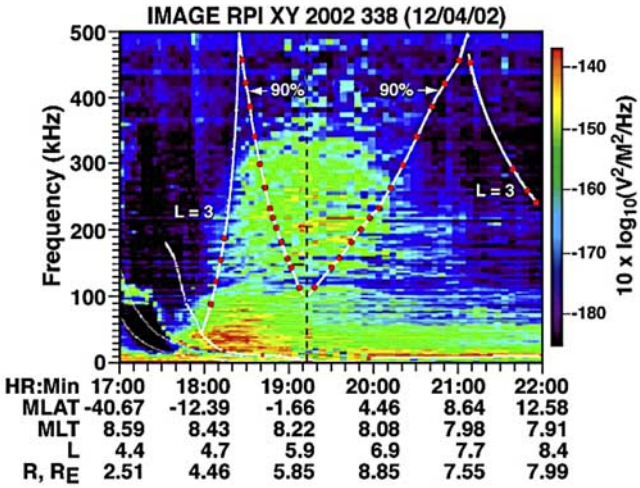

Figure 8. A frequency-time spectrogram of a KC event is shown. The inner V-shaped curve is derived from the 90th percentile curve shown in Figure 7. The white curves indicated by $L = 3$ were derived from a source plasmapause at an equatorial L-shell of 3, where the dipole model derived f_{ce} equals the spacing observed in the KC frequency bands for this event (see Figure 9). LMCT theory fails to quantitatively explain the observed latitudinal variation of KC with frequency for either case.

scatterplot of these in situ plasma density measurements versus L-shell. These density measurements, used in studies by *Fung et al.* [2001] and by *Garcia et al.* [2003], were made by hand-scaling of the upper hybrid resonance band, when detectable. *Benson et al.* [2004] discusses the reliability of the identification of the upper hybrid band and in using it to infer plasma densities. The red, green, and blue curves are the 90th, 50th, one percentile curves determined by binning the logarithm of the density measurements with L-shell. We used the 90th percentile curve (red) from Figure 7 in the beaming formula to derive a reasonable lower limit for the beaming angle as a function of KC wave frequency and its corresponding "source" L-shell. We emphasize that the 90th percentile curve does not represent a realistic plasmasphere shape but that it gives a reasonable estimate of the maximum plasma density that can occur at a specified equatorial L-shell. This curve can be used to place lower limits on the beaming angle at a given frequency.

[20] We overlaid these beaming angle lower limit curves on spectrograms of 80 KC radiation events for which there was not significant contamination from either AKR or type III solar bursts. Since these curves represent our estimates for the lower limits to the equatorial beaming angle, the LMCT predicts no significant radiation deep within the boundary defined by these curves for all frequencies that makeup the KC. Examples of KC radiation patterns, with these beaming angle lower limit curves (white curves) overlaid, are shown in Figures 2a–2d and in Figure 8. These beaming-angle lower limit curves move outward in latitude from the equator with increasing frequency and lie outside of the KC radiation pattern at the higher frequencies. Similarly, for all 80 events, the LMCT predicted beam centers were found to lay outside, or a best touch, the outer boundaries of the high-frequency portion of the observed radiation patterns. Therefore we conclude that LMCT fails to explain the high-frequency portion of these KC radiation patterns and therefore probably fails to explain their low-frequency extent also.

[21] In order to compare frequency components of the KC radiation patterns below ~150 kHz with LMCT, the location of the plasmapause at the source must be known. As discussed in the introduction, *Hashimoto et al.* [2005] used the plasmapause location observed ~90 min before encountering KC to infer the source position. We present one example (Figure 8) in which the source location is inferred by equating the observed harmonic spacing in the KC radiation (more apparent on the spectra shown in Figure 9) with a magnetic dipole model derived f_{ce} at the equatorial source. The equating of the observed harmonic spacing of NTC with a model equatorial f_{ce} has been used to remotely sense the plasmaspause location in studies of enhanced continuum by *Gough* [1982] and *Kasaba et al.* [1998]. The justification for equating harmonic spacing in NTC is based on one event at a sharp plasmapause where *Kurth* [1982] showed "a direct correspondence between the narrow band radio emissions and electron cyclotron harmonic waves near the upper hybrid frequency." We assume that such an equating of the observed harmonic spacing in radiation with f_{ce} at the equatorial source is also applicable in the KC frequency range.

[22] In our investigation of the event of Figures 8 and 9, we use 33 kHz as a representative spacing and equate it with the magnetic dipole model derived f_{ce} to determine an equatorial source location at 3 R_E. The curves labeled $L = 3$ are beam centers derived for a sharp plasmapause located an L-shell of 3 R_E. The left edge of the radiation pattern just touches left most $L = 3$ curve while the right edge lies completely inside of the right most $L = 3$ curve.

5. Discussion

[23] In our computations an azimuthally symmetric plasmasphere/plasmapause or 90th percentile plasma density

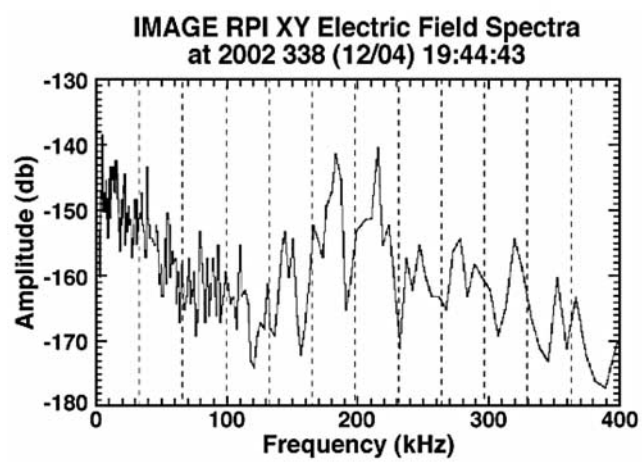

Figure 9. Combined X-Y antenna electric field frequency spectrum of KC emission bands is shown. The vertical dashed lines are spaced at the nf_{ce} for an assumed equatorial source location at 3 R_E. The IMAGE spacecraft is located at 6.6 R_E and 3.0° magnetic latitude.

model was used and the computations where made in the plane containing the source magnetic field direction and spacecraft position (the density gradient would also lie in this plane). This is obviously an extreme simplification of the real shape of the plasmapshere and plasmapause. One might wonder if rays launched at an azimuth angle about the magnetic field from the antidensity gradient direction in the equatorial plane might be focused more toward the equator than those emerging in the plane defined by the density gradient direction and the magnetic field direction. *Budden and Jones* [1987] have shown that the beaming angle out of the equatorial plane is not very sensitive to the azimuthal component of the emerging wave vector [see *Jones*, 1988, Figure 4; *Budden and Jones*, 1987, Figures 4 and 6]. Therefore the above assumption (spacecraft and source are in the same meridian plane) used to compute the synthetic spectrograms of the beam centers is reasonable.

[24] The beaming formula is only strictly valid for plasmas with a constant density gradient and uniform magnetic field. This approximation should also be very good for sources at realistic plasmapauses. In order to test the beaming formula, we performed cold plasma wave ray tracing in a model plasmasphere/plasmapause over a broad range of frequencies. We launched L-O mode waves very close to, but just outside, the radio window, terminating the ray trace 5 R_E away from the source. Since we know the model magnetic field direction at the equatorial plasmapause source and the source location and the location of the end point of the ray, we are able to compute a beaming angle for a set of ray-traced frequencies. Our cold plasma wave ray tracing derived beaming angles where found to be in close agreement with the angles given by the LMCT beaming formula, but they tended to be a degree or two larger than that given by the formula. Therefore cold plasma wave ray tracing from the radio window did not result in a ray propagating closer to the magnetic equator than that computed from the formula.

[25] In our cold plasma wave ray tracing model the density is constant along an *L*-shell near the magnetic equator. A density minimum along an *L*-shell at the equator could help to refract the emitted radiation back toward the equator. A density minimum at the equator will be small and gradual at best, but because the window is right at the plasma frequency the wave propagation could still be influenced by a small minimum. *Huang et al.* [2004] modeled the density variation along an *L*-shell by inverting ducted echoes detected by RPI and deduced a relatively flat density profile across the equator. Trapped particles at the equator could introduce a small density enhancement along an *L*-shell at the equator. *Olsen et al.* [1994] estimated that trapped distributions could contribute 5 to 20 cm^{-3} to the equatorial plasma density and this should mildly divert the LMCT beams away from the equator.

[26] *Budden* [1980, 1986] derives a formula [*Budden*, 1986, equation (21)] that gives the attenuation of the transmitted wave as a function of the angle of the emergent *L*-mode wave from the center of the window. Could *Z*-mode radiation illuminate the window in a systematic way such that the *L*-mode emerges from the window at an angle closer to the magnetic equator than the angle given by the beaming formula (given in the introduction, for which there is no attenuation) without experiencing significant attenuation? For example, in Figure 6 of *Hashimoto et al.* [2005] the latitude difference between beaming angles estimated from observation and LMCT theory is about 8° for frequencies of 100 and 200 kHz, and about 3.5° for the frequency 300 kHz. Using these offsets in latitude from the radio window center, with a plasma density gradient of -1333 m^{-4} at the source plasmapause at 3.9 R_E, gives an attenuation of -32 db, -170 db, and -88 db for these frequencies of 100, 200, and 300 kHz, respectively. So for frequencies greater than 100 kHz the waves would be attenuated by at least 3 orders magnitude upon transmission through the window. Therefore a systematic off center illumination of the radio window by incident *Z*-mode radiation seems and unlikely explanation for the discrepancy between observation and LMCT in the KC frequency range. As mentioned in section 1, there are a number of mechanisms that can contribute to broadening and smearing of the LMCT beams, but it is difficult to come up with mechanisms using LMCT that would focus these beams toward the equator.

6. Conclusion

[27] Using 80 observations of KC radiation patterns detected by the RPI on the IMAGE spacecraft, the latitudinal variation of these radiation patterns is compared with the predictions of LMCT. Six of these comparisons are presented in this paper. Because the location and shape of the plasmapause at the source cannot be simultaneously determined with the KC observations, we estimated the minimum frequency-dependent beaming angle possible using LMCT based on a statistical upper limit plasma density versus *L*-shell profile. This density versus *L*-shell profile was based on the 90th percentile plasma density versus *L*-shell curve derived from over 40,000 in situ measurements of the upper hybrid resonance frequency made over the first 3 years of the IMAGE mission. For all cases, starting at frequencies approximately >150 kHz, the model beam center was found to lie just within the radiation pattern or outside it, that is, at latitudes farther away from the equator. Unrealistic peak densities are required at the source *L*-shell locations to force the beam centers to lie deep within the observed radiation patterns. We present these results as strong evidence that LMCT cannot be used to explain KC. In order to explain the latitudinal location of the high-frequency end of these KC radiation patterns, a theory is required in which these frequencies are beamed at equatorial angles that are much smaller than the predictions of LMCT. *Hashimoto et al.* [2005], analyzing one radiation pattern detected by CRRES, reached the same conclusion. Also in our investigation, one case is presented, in which the source location was inferred by equating the harmonic spacing in the KC radiation pattern with the model electron cyclotron frequency at the source. The LMCT model beams, for this source location, were found to lie outside of the radiation pattern at all frequencies, again consistent with the conclusion of *Hashimoto et al.* [2005]. In addition, a survey of KC observations by IMAGE in MLT is presented in which the probability of occurrence peaks in both the dawn and evening sectors.

[28] **Acknowledgments.** The authors thank L. Garcia and S. F. Fung for providing the in situ plasma frequency measurements used in this study. The research performed was supported by the NASA Guest Investigator Program grant NNX07AC10G (Multi-Spacecraft Study of Escaping Continuum). The work at the University of Massachusetts-Lowell was supported by NASA under subcontracts to Southwest Research Institute under NASA contract NASW-97002.

[29] Zuyin Pu thanks Robert Benson and another reviewer for their assistance in evaluating this paper.

References

Benson, R. F., P. A. Webb, J. L. Green, L. Garcia, and B. W. Reinisch (2004), Magnetospheric electron densities inferred from upper-hybrid band emissions, *Geophys. Res. Lett.*, *31*, L20803, doi:10.1029/2004GL020847.

Budden, K. G. (1980), The theory of radio windows in the ionosphere and magnetosphere, *J. Atmos. Terr. Phys.*, *42*, 287–298.

Budden, K. G. (1986), The theory of radio windows in the ionosphere and magnetosphere – II, *J. Atmos. Terr. Phys.*, *48*, 633–641.

Budden, K. G., and D. Jones (1987), Conversion of electrostatic upper hybrid emissions to electromagnetic O and X mode waves in the Earth's magnetosphere, *Ann. Geophys.*, *5A*, 21–28.

Burch, J. L. (Ed.) (2000), The IMAGE mission, *Space Sci. Rev.*, *91*, 1–2.

Carpenter, D. L., and R. R. Anderson (1992), An ISEE/whistler model of equatorial electron density in the magnetosphere, *J. Geophys. Res.*, *97*, 1097–1108.

Fung, S. F., L. N. Garcia, J. L. Green, D. L. Gallagher, D. L. Carpenter, B. W. Reinisch, I. A. Galkin, G. Khmyrov, and B. R. Sandel (2001), Plasmaspheric electron density distributions sampled by Radio Plasma Imager on the IMAGE satellite, *Eos Trans. AGU*, *82*(47), Fall Meet. Suppl., Abstract SM11A-0771.

Galkin, I., B. W. Reinisch, G. Grinstein, G. Khmyrov, A. Kozlov, X. Huang, and S. F. Fung (2004), Automated exploration of the radio plasma imager data, *J. Geophys. Res.*, *109*, A12210, doi:10.1029/2004JA010439.

Gallagher, D. L., P. D. Craven, and R. H. Comfort (2000), Global core plasma model, *J. Geophys. Res.*, *105*, 18,819–18,834.

Garcia, L. N., S. F. Fung, J. L. Green, S. A. Boardsen, B. R. Sandel, and B. W. Reinisch (2003), Observations of the latitudinal structure of plasmaspheric convection plumes by IMAGE-RPI and EUV, *J. Geophys. Res.*, *108*(A8), 1321, doi:10.1029/2002JA009496.

Gough, M. P. (1982), Non-thermal continuum emissions associated with electron injections: remote plasmapause sounding, *Planet. Space Sci.*, *30*, 657–668.

Green, J. L., and S. A. Boardsen (2006), Kilometric continuum radiation, *Radio Sci. Bull.*, *318*, 34–41.

Green, J. L., B. R. Sandel, S. F. Fung, D. L. Gallagher, and B. W. Reinisch (2002), On the origin of kilometric continuum, *J. Geophys. Res.*, *107*(A7), 1105, doi:10.1029/2001JA000193.

Green, J. L., S. Boardsen, S. F. Fung, H. Matsumoto, K. Hashimoto, R. R. Anderson, B. R. Sandel, and B. W. Reinisch (2004), Association of kilometric continuum radiation with plasmaspheric structures, *J. Geophys. Res.*, *109*, A03203, doi:10.1029/2003JA010093.

Gurnett, D. A. (1975), The Earth as a radio source: The nonthermal continuum, *J. Geophys. Res.*, *80*, 2751–2763.

Gurnett, D. A., and R. A. Shaw (1973), Electromagnetic radiation trapped in the magnetosphere above the plasma frequency, *J. Geophys. Res.*, *78*, 8136–8148.

Hashimoto, K., W. Calvert, and H. Matsumoto (1999), Kilometric continuum detected by Geotail, *J. Geophys. Res.*, *104*, 28,645–28,656.

Hashimoto, K., R. R. Anderson, J. L. Green, and H. Matsumoto (2005), Source and propagation characteristics of kilometric continuum observed with multiple satellites, *J. Geophys. Res.*, *110*, A09229, doi:10.1029/2004JA010729.

Hashimoto, K., J. L. Green, R. R. Anderson, and H. Matsumoto (2006), Review of kilometric continuum, in *Geospace Electromagnetic Waves and Radiation*, *Lect. Not. in Phys.*, vol. 687, edited by J. W. LaBelle and R. A. Treumann, pp. 37–54, Springer, New York.

Horne, R. B. (1989), Path-integrated growth of electrostatic waves: The generation of terrestrial myriametric radiation, *J. Geophys. Res.*, *94*, 8895–8909.

Huang, X., B. W. Reinisch, P. Song, P. Nsumei, J. L. Green, and D. L. Gallagher (2004), Developing an empirical density model of the plasmasphere using IMAGE/RPI observations, *Adv. Space Res.*, *33*, 829–832.

Jones, D. (1976), Source of terrestrial nonthermal radiation, *Nature*, *260*, 686–689.

Jones, D. (1980), Latitudinal beaming of planetary radio emissions, *Nature*, *288*, 225–229.

Jones, D. (1981), Beaming of terrestrial myriametric radiation, *Adv. Space Res.*, *1*, 373–376.

Jones, D. (1988), Planetary radio emissions from low magnetic latitudes: Observations and theories, in *Planetary Radio Emissions II*, edited by H. O. Rucker, S. J. Bauer, and B.-M. Pedersen, pp. 255–293, Austrian Acad. of Sci., Vienna.

Jones, D., W. Calvert, D. A. Gurnett, and R. L. Huff (1987), Observed beaming of terrestrial myiametric radiation, *Nature*, *328*, 391–395.

Kasaba, Y., H. Matsumoto, K. Hashimoto, R. R. Anderson, J.-L. Bougeret, M. L. Kaiser, X. Y. Wu, and I. Nagano (1998), Remote sensing of the plasmapause during substorms: Geotail observation of nonthermal continuum enhancement, *J. Geophys. Res.*, *103*, 20,389–20,405.

Kurth, W. S. (1982), Detailed observations of the source of terrestrial narrowband electromagnetic radiation, *Geophys. Res. Lett.*, *9*, 1341–1344.

Kurth, W. S., D. A. Gurnett, and R. R. Anderson (1981), Escaping nonthermal continuum radiation, *J. Geophys. Res.*, *86*, 5519–5531.

Moldwin, M. B., L. Downward, H. K. Rassoul, R. Amin, and R. R. Anderson (2002), A new model of the location of the plasmapause: CRRES results, *J. Geophys. Res.*, *107*(A11), 1339, doi:10.1029/2001JA009211.

Morgan, D. D., and D. A. Gurnett (1991), The source location and beaming of terrestrial continuum radiation, *J. Geophys. Res.*, *96*, 9595–9613.

Olsen, R. C., L. J. Scott, and S. A. Boardsen (1994), Comparison between Liouville's theorem and observed latitudinal distributions of trapped ions in the plasmapause region, *J. Geophys. Res.*, *99*, 2191–2204.

Reinisch, B. W., et al. (2000), The Radio Plasma Imager investigation on the IMAGE spacecraft, *Space Sci. Rev.*, *91*, 319–359.

S. A. Boardsen, Heliophysics Science Division, NASA Goddard Space Flight Center, Code 674.0, Greenbelt, MD 20771, USA. (scott.a.boardsen@nasa.gov)

J. L. Green, Planetary Sciences Division, NASA Headquarters, 300 E Street, SW, MS 3274, Washington, DC 20546-0001, USA.

B. W. Reinisch, Center for Atmospheric Research, University of Massachusetts-Lowell, 600 Suffolk Street, 3rd Floor South, Lowell, MA 01854, USA.